Imaging the competition between growth and production of self-assembled lipid droplets at the single-cell level

Imaging the competition between growth and production of self-assembled lipid droplets at the single-cell level

Vasdekis, A., Alanazi, H., Silverman, A., Canul, A., Dohnalkova, A., et al.

A. E. Vasdekis, H. Alanazi, A. M. Silverman, A. J. Canul, A. C. Dohnalkova, J. B. Cliff, G. Stephanopoulos, "Imaging the competition between growth and production of self-assembled lipid droplets at the single-cell level," Proc. SPIE 11060, Optical Methods for Inspection, Characterization, and Imaging of Biomaterials IV, 110600E (21 June 2019); doi: 10.1117/12.2531007

SPIE.

Event: SPIE Optical Metrology, 2019, Munich, Germany

Imaging the competition between growth and production of self-assembled lipid droplets at the single-cell level

A. E. Vasdekis[1], H. Alanazi[1], A. M. Silverman[2], A. J. Canul[1], A. C. Dohnalkova[3], J. B. Cliff[3], G. Stephanopoulos[2]

[1] Department of Physics, University of Idaho, Moscow, ID 83844, USA.

[3] Environmental Molecular Sciences Laboratory, Pacific Northwest National Laboratory, Richland, WA 99354, USA.

[2] Department of Chemical Engineering, Massachusetts Institute of Technology, Cambridge, MA 02139, USA.

ABSTRACT

Several biotechnologies are currently available to quantify how cells allocate resources between growth and carbon storage, such as mass spectrometry. However, such biotechnologies require considerable amounts of cellular biomass to achieve adequate signal-to-noise ratio. In this way, existing biotechnologies inevitably operate in a 'population averaging' mode and, as such, they cannot unmask how cells allocate resources between growth and storage in a high-throughput fashion with single-cell, or subcellular resolution. This methodological limitation inhibits our fundamental understanding of the mechanisms underlying resource allocations between different cellular metabolic objectives. In turn, this knowledge gap also pertains to systems biology effects, such as cellular noise and the resulting cell-to-cell phenotypic heterogeneity, which could potentially lead to the emergence of distinct cellular subpopulations even in clonal cultures exposed to identical growth conditions. To address this knowledge gap, we applied a high-throughput quantitative phase imaging strategy. Using this strategy, we quantified the optical-phase of light transmitted through the cell cytosol and a specific cytosolic organelle, namely the lipid droplet (LD). With the aid of correlative secondary ion mass spectrometry (NanoSIMS) and transmission electron microscopy (TEM), we determined the protein content of different cytosolic organelles, thus enabling the conversion of the optical phase signal to the corresponding dry density and dry mass. The high-throughput imaging approach required only 2 μL of culture, yielding more than 1,000 single, live cell observations per tested experimental condition, with no further processing requirements, such as staining or chemical fixation.

Keywords: interferometry, bioimaging, single-cell, metabolism, trade-offs

1. INTRODUCTION

Most eukaryotes store excess carbon into lipid droplets (LDs), namely self-assembled, spherical organelles with significant implications in human health and bioengineering [1]. While substantial improvements in our fundamental understanding [2-4] and engineering [5-7] of lipid metabolism has been achieved in recent years, we still lack the mechanistic insight of how individual cells in a clonal population allocate resources between carbon assimilation into LDs and other cellular

Optical Methods for Inspection, Characterization, and Imaging of Biomaterials IV, edited by Pietro Ferraro, Simonetta Grilli, Monika Ritsch-Marte, Christoph K. Hitzenberger, Proc. of SPIE Vol. 11060, 110600E
 · doi: 10.1117/12.2531007

objectives, such as cellular growth that has been tightly optimized under selective pressure [8]. To this end, conventional biotechnologies that screen for lipid accumulation and growth operate in a population-averaging mode [5]. As such, these methods inevitably lack the required single-cell and subcellular resolution and are thus unable to detect differences between individual cells and the inevitable emergence of metabolic subpopulations due to infrequent mutations, cytosolic stochastic phenomena, and extracellular perturbations [9-12]. These metabolic subpopulations may seem insignificant but can have a substantial impact on the overall population response, including the production levels of bioentities of industrial interest, as well as stress-response, such as antibiotic treatment [13, 14].

A common approach to screen cell metabolism with subcellular resolution in live cells is to use optical microscopy. However, conventional, volumetric, microscopy informs solely about cell and LD size, namely parameters that contribute only partially to the cell's enthalpy and Gibb's free energy. Further, volumetric optical methods assume that cellular and LD densities are homogenous between individual cells and independent of growth conditions. This assumption, however, has not been yet validated. Therefore, and despite the considerable ongoing progress in single-cell methods [15, 16], imaging resource allocations in various metabolic objectives and especially lipid accumulation and growth with subcellular resolution remains an important target.

To meet this target, we adopted interferometric, quantitative-phase imaging [17-19] using lipid biogenesis in the oleaginous yeast *Yarrowia lipolytica* as a model process [5]. By capturing the optical-phase delay ($\Delta\Phi$) induced by the cell cytosol and LDs separately, we attained their corresponding dry-weights (DW) with the aid of Nanoscale Secondary Ion Mass Spectrometry (NanoSIMs) and Transmission Electron Microcopy (TEM). In this way, we improved the precision of conventional, volumetric imaging by more than 50% in quantifying how resources are allocated to growth and lipid production [20]. In the following sections, we detail our bioimaging approach, as well as the resulting precision quantification of resource allocations to the accumulation of lipids and cellular growth.

2. BIOIMAGING

We employed the spatial light interference microscopy modality [17] to acquire approximately 1000 single-cell quantitative-phase images using only 2 μL of a growing culture per tested experimental condition. Subsequently, we localized the cell contour through the increased $\Delta\Phi$ of the cell cytosol without any fluorescent labelling [21]. Contrary to cell-segmentation [21], however, the LD-to-cytosol contrast was inadequate for automated high-throughput LD localization. To overcome this shortcoming and enable high-throughput LD detection from quantitative-phase images, we additionally collected conventional phase-contrast intensity images, where the non-diffracted wavefront [17] was further modulated by an additional phase-delay of $\pi/2$ and π [11]. Cross-correlating the resulting images, any non-specific contributions to the LD localization were suppressed, yielding greater than 98% correlation with fluorescence, as we further detail in a recent publication [20].

Following the localization of the cell cytosol and LDs, we subsequently converted their corresponding phase-delay signal to dry-mass (DM) values, by hypothesizing that the cell cytosol is primarily comprised of proteins and nucleic acids, dispersed with LDs that are loaded with triacylglycerides (TAGs) at a negligible protein content. We confirmed this hypothesis by characterizing the cytosolic and LD elemental composition with nanoscale secondary ion mass spectrometry (NanoSIMS). As further detailed in [20], we indeed found the cytosol to be uniformly comprised of naturally abundant nitrogen (^{14}N) following the exposure to U-^{13}C glucose at various carbon-to-nitrogen ratios (C/N) and durations using two independent cultures. To a similar end, LDs, which were co-localized by Transmission Electron Microscopy (TEM) and NanoSIMS, were found to be comprised primarily of ^{13}C with negligible ^{14}N content.

To finalize the conversion of the acquired phase-delay value of the cell cytosol ($\Delta\Phi_{cytosol}$) to the corresponding cellular biomass, we employed the protein refractive index increment, given that the cell cytosol can be approximated as an aqueous protein solution [22]. In contrast, a similar increment cannot be directly applied to LDs given that these pertain to self-assembled glycerolipids, which for *Y. lipolytica* are relatively homogeneous with approximately 95% triacylglycerides (TAGs). To address this, we employed the Clausius-Mossotti equation to convert the experimentally determined LD refractive index to the corresponding number-density of TAG molecules, and thus the LD dry-density. To this end, we considered a mixture of triolein, stearin, tripalmitin, trilinolein, and tripalmitolein and calculated the mixture TAG polarizability parameter for *Y. lipolytica* specifically. As we recently reported [20], the TAG mixture polarizability parameter does not vary significantly under typical growth conditions.

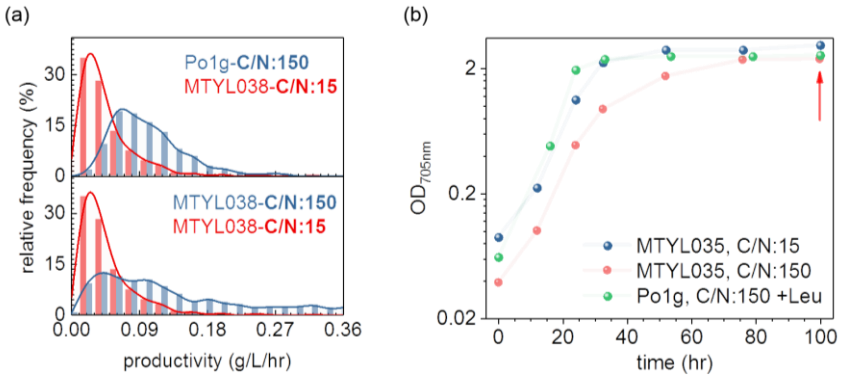

Figure 1: (a) Comparison of the $MTYL038_{15}$ single-cell productivity distribution with $MTYL038_{150}$ (lower) and $Po1g_{150}$ (upper). Cells were grown for 100 hr each in YSM medium. The YPD and YSM media formulations are further detailed in [20]. All precultures were stored in YPD agarose (Invitrogen) plates at 4°C and passed twice in YPD medium. The second passage was performed at 50x dilution, followed by a 24 hr long growth in YPD, centrifugation at 2000 rpm, and washing in YSM three times, prior to transferring to 40 ml Falcon tubes containing 20 ml of the YSM medium. The Falcon tubes enabled limited oxygen exchange during batch growth. All growth experiments were performed in a shaking incubator at 200 rpm and a temperature of 28°C. Growth curves were determined via optical density measurements using a custom-built light transmission system utilizing a 705 nm diode laser and 0.5 ml samples in 1 ml polystyrene cuvettes. **(b)** Growth curves represented through optical density at 705 nm for all experimental conditions presented in (a).

3. RESULTS

3.1. Precision assessment

For various growth conditions and strains, we found that the LD volume correlated poorly with the TAG number-density, while exhibiting increased variance (or heterogeneity) between individual cell observations. Similarly, the cell DW-volume relationship exhibited high variability and occasionally scaled inversely, yielding a relatively poor correlation between these two parameters [20]. Both the increased variance and weak correlations in the density-size relationship for both LDs and non-TAG cellular biomass unravel key precision limitations of conventional, volumetric, microscopy in phenotyping lipid accumulation and growth. These limitations pertain both to precision quantification of the average population response, as well as the underlying cell-to-cell phenotypic heterogeneity and cellular noise, which for *Y. lipolytica* specifically, we determined an average error of 55% with significant differences between specific strain and growth-conditions [20].

To further assess the precision improvement of quantitative-phase imaging in comparison to population-averaging biotechnologies, we compared the lipid production levels (i.e., the amount of TAG produced per unit time) of two genetically similar *Y. lipolytica* strains (MTYL038 and Po1g). Specifically, we compared the MTYL038 productivity at a carbon-to-nitrogen ratio (C/N) of 15 ($MTYL038_{15}$) with the productivity of MTYL038 and Po1g at C/N:150 ($MTYL038_{150}$

and Po1g$_{150}$, **Fig. 1**). Using the Kolmogorov–Smirnov (KS) statistic to account for cell-to-cell heterogeneity, we determined that the [MTYL038$_{15}$–Po1g$_{150}$] pair exhibited the largest phenotypic distance. In contrast, the largest Euclidian distance, which simulates the readout of population-averaging methods, was with the [MTYL038$_{15}$–MTYL038$_{150}$] pair. This inconsistency is due to the enhanced strain-classification precision of single-cell mass-balance phenotyping, which objectively captures the different origins of productivity improvement in each strain, namely: improvement was driven by overproducing subpopulations for MTYL038$_{150}$, while for Po1g$_{150}$ by a 4-fold productivity increase of its most likely phenotypes (**Fig. 1**).

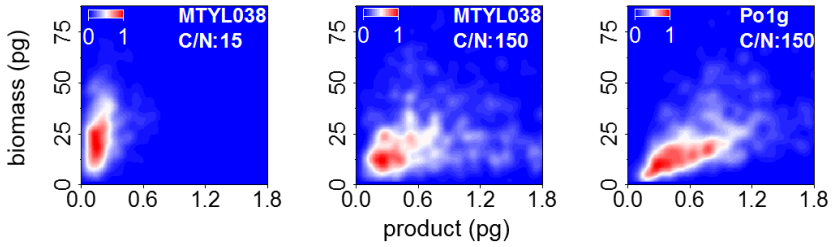

Figure 2: 2D probability distributions for biomass and product allocations for MTYL03815, Po1g150 and MTYL03815.

3.2. Competition between LD accumulation and growth

To visualize the competition of resource allocations between lipid accumulation and growth, we performed a single-cell multivariate analysis [23], as illustrated in **Fig. 2**. This analysis enabled direct quantification of the corresponding probability distributions directly in a 2D metabolic space under various experimental conditions. Specifically, we found that MTYL038$_{15}$ allocated resources primarily to growth, as anticipated due to the low C/N ratio in the medium formulation. In contrast, Po1g$_{150}$ displayed a metabolic shift towards high-lipid and low-biomass microstates. A similar behavior was observed for MTYL038$_{150}$, albeit this transition exhibited only sporadic high-product and low-biomass subpopulations, indicative of reduced robustness during lipid accumulation. Further analysis during specific timepoints for MTYL038$_{150}$ revealed that during late stationary phase (>70 hr, **Fig. 3**), both biomass and product decreased. This form of decrease indicates the onset of an autophagy-based central catabolic process for both metabolic objectives, which do not necessarily exhibit the same rates and same levels of cellular noise. Overall, quantitative-phase imaging uniquely revealed that the competition of resource allocations between growth and LD content pertains both during nutrient rich and starvation conditions.

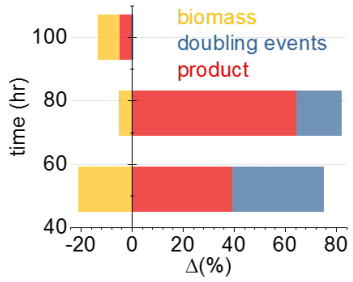

Figure 3: The time-dependent change (Δ%) of cell biomass, product, and cell-doubling for MTYL038$_{150}$.

4. CONCLUSIONS

In summary, we report single-cell quantitative-phase imaging and its use in high-throughput screening of resource allocations between lipid accumulation and growth. Quantitative-phase imaging uniquely differentiated cell biomass from intracellular metabolites in single-cells, otherwise impossible to accomplish with conventional microscopy, population-

averaging biotechnologies, and alternative single-cell mass characterization methods [24, 25]. The high-throughput imaging approach required only 2 µL of culture, yielding more than 1,000 single live cell observations with no further processing requirements, such as staining or chemical fixation. Overall, quantitative phase imaging precisely quantified how resources are allocated between growth and carbon storage at the single-cell level. Detailed analysis of our imaging results indicated that not all cells follow the same resource allocation strategy. In contrast, distinct metabolic subpopulations emerge with important implications in the overall population production of lipids. Importantly, these results were not possible to attain with population-averaging biotechnologies. Similarly, conventional, volumetric microscopy was unable to precisely quantify the competition between growth and lipid production through LD self-assembly due to significant biomass dry-density differences between individual cells. The described high-throughput quantitative-phase imaging strategy has several potential applications in bioengineering, beyond lipid biogenesis as probed by way of example here.

5. ACKNOWLEDGMENTS

A.E.V. acknowledges support from the U.S. Department of Energy, Office of Science, Office of Biological and Environmental Research (DE-SC0019249), the Leonard Halland Fund for equipment acquisition and support during preliminary investigations, as well as partial support from the National Institutes of Health (P20GM104420) during preliminary investigations. G.S. acknowledges support from the U.S. Department of Energy, Office of Science, Office of Biological and Environmental Research (DE-SC0008744). Part of the research was performed using EMSL at Pacific Northwest National Laboratory (Proposal ID 49084), a DOE Office of Science Use Facility sponsored by the Office of Biological and Environmental Research.

6. REFERENCES

1. Guo, Y., et al., *Lipid droplets at a glance.* Journal of Cell Science, 2009. **122**(6): p. 749-752.

2. Khor, V.K., W.J. Shen, and F.B. Kraemer, *Lipid droplet metabolism.* Curr Opin Clin Nutr Metab Care, 2013. **16**(6): p. 632-7.

3. Zhang, J., Y. Lan, and S. Sanyal, *Modulation of Lipid Droplet Metabolism-A Potential Target for Therapeutic Intervention in Flaviviridae Infections.* Frontiers in microbiology, 2017. **8**: p. 2286-2286.

4. Walther, T.C. and R.V.F. Jr., *Lipid Droplets and Cellular Lipid Metabolism.* Annual Review of Biochemistry, 2012. **81**(1): p. 687-714.

5. Qiao, K., et al., *Lipid production in Yarrowia lipolytica is maximized by engineering cytosolic redox metabolism.* Nat Biotech, 2017. **35**(2): p. 173-177.

6. Tai, M. and G. Stephanopoulos, *Engineering the push and pull of lipid biosynthesis in oleaginous yeast Yarrowia lipolytica for biofuel production.* Metab Eng, 2013. **15**: p. 1-9.

7. Liang, M.H. and J.G. Jiang, *Advancing oleaginous microorganisms to produce lipid via metabolic engineering technology.* Prog Lipid Res, 2013. **52**(4): p. 395-408.

8. Stephanopoulos, G. and J.J. Vallino, *Network rigidity and metabolic engineering in metabolite overproduction.* Science, 1991. **252**(5013): p. 1675-81.

9. Elowitz, M.B., et al., *Stochastic Gene Expression in a Single Cell.* Science, 2002. **297**(5584): p. 1183-1186.

10. Cai, L., N. Friedman, and X.S. Xie, *Stochastic protein expression in individual cells at the single molecule level.* Nature, 2006. **440**(7082): p. 358-362.

11. Vasdekis, A.E., A.M. Silverman, and G. Stephanopoulos, *Origins of Cell-to-Cell Bioprocessing Diversity and Implications of the Extracellular Environment Revealed at the Single-Cell Level.* Scientific Reports, 2015. **5**: p. 17689.

12. van Dijk, D., et al., *Slow-growing cells within isogenic populations have increased RNA polymerase error rates and DNA damage.* Nature Communications, 2015. **6**: p. 7972.

13. Xiao, Y., et al., *Exploiting nongenetic cell-to-cell variation for enhanced biosynthesis.* Nat Chem Biol, 2016. **12**(5): p. 339-344.

14. Balaban, N.Q., et al., *Bacterial Persistence as a Phenotypic Switch.* Science, 2004.

15. Gawad, C., W. Koh, and S.R. Quake, *Single-cell genome sequencing: current state of the science.* Nat Rev Genet, 2016. **17**(3): p. 175-188.

16. Zenobi, R., *Single-Cell Metabolomics: Analytical and Biological Perspectives.* Science, 2013. **342**(6163).

17. Kim, T., et al., *White-light diffraction tomography of unlabelled live cells.* Nat Photon, 2014. **8**(3): p. 256-263.

18. Barer, R., *Interference Microscopy and Mass Determination.* Nature, 1952. **169**(4296): p. 366-367.

19. Kim, K., et al., *Three-dimensional label-free imaging and quantification of lipid droplets in live hepatocytes.* Scientific Reports, 2016. **6**: p. 36815.

20. Vasdekis, A., et al., *Eliciting the impacts of cellular noise on metabolic trade-offs by quantitative mass imaging.* Nature Communications, 2019. **10**(1): p. 848.

21. Alanazi, H., et al., *Robust microbial cell segmentation by optical-phase thresholding with minimal processing requirements.* Cytometry Part A, 2017. **91**(5): p. 443-449.

22. Zangle, T.A. and M.A. Teitell, *Live-cell mass profiling: an emerging approach in quantitative biophysics.* Nat Methods, 2014. **11**(12): p. 1221-8.

23. Altschuler, S.J. and L.F. Wu, *Cellular Heterogeneity: Do Differences Make a Difference?* Cell, 2010. **141**(4): p. 559-563.

24. Stevens, M.M., et al., *Drug sensitivity of single cancer cells is predicted by changes in mass accumulation rate.* Nat Biotech, 2016. **34**(11): p. 1161-1167.

25. Martinez-Martin, D., et al., *Inertial picobalance reveals fast mass fluctuations in mammalian cells.* Nature, 2017. **550**(7677): p. 500-505.